Weak-Localization Magnetoresistance and Valley Symmetry in Graphene

E. McCann,[1] K. Kechedzhi,[1] Vladimir I. Fal'ko,[1] H. Suzuura,[2] T. Ando,[3] and B. L. Altshuler[4]

[1]*Department of Physics, Lancaster University, Lancaster, LA1 4YB, United Kingdom*
[2]*Division of Applied Physics, Graduate School of Engineering, Hokkaido University, Sapporo 060-8628, Japan*
[3]*Department of Physics, Tokyo Institute of Technology, 2-12-1 Ookayama, Meguro-ku, Tokyo 152-8551, Japan*
[4]*Physics Department, Columbia University, 538 West 120th Street, New York, New York 10027, USA*

(Received 2 April 2006; published 5 October 2006)

Because of the chiral nature of electrons in a monolayer of graphite (graphene) one can expect weak antilocalization and a positive weak-field magnetoresistance in it. However, trigonal warping (which breaks $\mathbf{p} \to -\mathbf{p}$ symmetry of the Fermi line in each valley) suppresses antilocalization, while intervalley scattering due to atomically sharp scatterers in a realistic graphene sheet or by edges in a narrow wire tends to restore conventional negative magnetoresistance. We show this by evaluating the dependence of the magnetoresistance of graphene on relaxation rates associated with various possible ways of breaking a "hidden" valley symmetry of the system.

DOI: 10.1103/PhysRevLett.97.146805 PACS numbers: 73.63.Bd, 71.70.Di, 73.43.Cd, 81.05.Uw

The chiral nature [1–4] of quasiparticles in graphene (monolayer of graphite), which originates from its honeycomb lattice structure and is revealed in quantum Hall effect measurements [5,6], is attracting a lot of interest. In recently developed graphene-based transistors [5,6] the electronic Fermi line consists of two tiny circles [7] surrounding corners $\mathbf{K}_\pm$ of the hexagonal Brillouin zone [8], and quasiparticles are described by 4-component Bloch functions $\Phi = [\phi_{\mathbf{K}_+,A}, \phi_{\mathbf{K}_+,B}, \phi_{\mathbf{K}_-,B}, \phi_{\mathbf{K}_-,A}]$, which characterize electronic amplitudes on two crystalline sublattices (A and B), and the Hamiltonian

$$\hat{H} = v\Pi_z \otimes \boldsymbol{\sigma}\mathbf{p} - \mu[\sigma_x(p_x^2 - p_y^2) - 2\sigma_y p_x p_y]. \quad (1)$$

Here, we use direct products of Pauli matrices $\sigma_{x,y,z}$, $\sigma_0 \equiv \hat{1}$ acting in the sublattice space (A, B) and $\Pi_{x,y,z}$, $\Pi_0 \equiv \hat{1}$ acting in the valley space ($\mathbf{K}_\pm$) to highlight the form of $\hat{H}$ in the nonequivalent valleys [8]. Near the center of each valley electron dispersion is determined by the Dirac-type part $v\boldsymbol{\sigma}\mathbf{p}$ of $\hat{H}$. It is isotropic and linear. For the valley $\mathbf{K}_+$ the electronic excitations with momentum $\mathbf{p}$ have energy vp and are chiral with $\boldsymbol{\sigma}\mathbf{p}/p = 1$, while for holes the energy is $-vp$ and $\boldsymbol{\sigma}\mathbf{p}/p = -1$. In the valley $\mathbf{K}_-$, the chirality is inverted: it is $\boldsymbol{\sigma}\mathbf{p}/p = -1$ for electrons and $\boldsymbol{\sigma}\mathbf{p}/p = 1$ for holes. The quadratic term in Eq. (1) violates the isotropy of the Dirac spectrum and causes a weak trigonal warping.

Because of the chirality of electrons in a graphene-based transistor, charges trapped in the substrate or on its surface cannot scatter carriers in exactly the backwards direction [2,7], provided that they are remote from the graphene sheet by more than the lattice constant. In the theory of quantum transport [9], the suppression of backscattering is associated with weak antilocalization (WAL) [10]. For purely potential scattering, possible WAL in graphene has recently been related to the Berry phase π specific to the Dirac fermions, though it has also been noticed that conventional weak localization (WL) may be restored by intervalley scattering [11,12].

In this Letter we show that the WL magnetoresistance (MR) in graphene directly reflects the degree of valley symmetry breaking by the warping term in the free-electron Hamiltonian (1) and by atomically sharp disorder. To describe the valley symmetry, we introduce two sets of 4×4 Hermitian matrices: "isospin" $\vec{\Sigma} = (\Sigma_x, \Sigma_y, \Sigma_z)$ and "pseudospin" $\vec{\Lambda} = (\Lambda_x, \Lambda_y, \Lambda_z)$. These are defined as

$$\Sigma_x = \Pi_z \otimes \sigma_x, \quad \Sigma_y = \Pi_z \otimes \sigma_y, \quad \Sigma_z = \Pi_0 \otimes \sigma_z, \quad (2)$$

$$\Lambda_x = \Pi_x \otimes \sigma_z, \quad \Lambda_y = \Pi_y \otimes \sigma_z, \quad \Lambda_z = \Pi_z \otimes \sigma_0, \quad (3)$$

and form two mutually independent algebras, $[\vec{\Sigma}, \vec{\Lambda}] = 0$,

$$[\Sigma_{s_1}, \Sigma_{s_2}] = 2i\varepsilon^{s_1 s_2 s}\Sigma_s, [\Lambda_{l_1}, \Lambda_{l_2}] = 2i\varepsilon^{l_1 l_2 l}\Lambda_l,$$

which determine two commuting subgroups of the group U_4 of unitary transformations [13] of a 4-component Φ: an isospin (sublattice) group $\mathrm{SU}_2^\Sigma \equiv \{e^{ia\vec{n}\vec{\Sigma}}\}$ and a pseudospin (valley) group $\mathrm{SU}_2^\Lambda \equiv \{e^{ib\vec{n}\cdot\vec{\Lambda}}\}$.

The operators $\vec{\Sigma}$ and $\vec{\Lambda}$ help us to represent the electron Hamiltonian in weakly disordered graphene as

$$\hat{H} = v\vec{\Sigma}\mathbf{p} + \hat{h}_w + \hat{I}u(\mathbf{r}) + \sum_{s,l=x,y,z} \Sigma_s \Lambda_l u_{s,l}(\mathbf{r}),$$

$$\text{where} \quad \hat{h}_w = -\mu\Sigma_x(\vec{\Sigma}\mathbf{p})\Lambda_z\Sigma_x(\vec{\Sigma}\mathbf{p})\Sigma_x. \quad (4)$$

The Dirac part of $\hat{H}$ in Eq. (4), $v\vec{\Sigma}\mathbf{p}$, and potential disorder $\hat{I}u(\mathbf{r})$ [$\hat{I}$ is a 4×4 unit matrix and $\langle u(\mathbf{r})u(\mathbf{r}')\rangle = u^2\delta(\mathbf{r} - \mathbf{r}')$] do not contain pseudospin operators Λ_l; i.e., they remain invariant under the group SU_2^Λ transformations. Since $\vec{\Sigma}$ and $\vec{\Lambda}$ change sign under the time inversion [14], the products $\Sigma_s\Lambda_l$ are $t \to -t$ invariant and, together with $\hat{I}$, can be used as a basis to represent nonmagnetic static disorder. Below, we assume that remote charges

dominate the elastic scattering rate, $\tau^{-1} \approx \tau_0^{-1} \equiv \pi\gamma u^2/\hbar$, where $\gamma = p_F/(2\pi\hbar^2 v)$ is the density of states of quasiparticles per spin in one valley. All other types of disorder which originate from atomically sharp defects [15] and break the SU_2^Λ pseudospin symmetry are included in a time-inversion-symmetric [14] random matrix $\Sigma_s \Lambda_l u_{s,l}(\mathbf{r})$. Here, $u_{z,z}(\mathbf{r})$ describes different on-site energies on the A and B sublattices. Terms with $u_{x,z}(\mathbf{r})$ and $u_{y,z}(\mathbf{r})$ take into account fluctuations of $A \rightleftarrows B$ hopping, whereas $u_{s,x}(\mathbf{r})$ and $u_{s,y}(\mathbf{r})$ generate intervalley scattering. In addition, warping term $\hat{h}_w$ not only breaks $\mathbf{p} \to -\mathbf{p}$ symmetry of the Fermi lines within each valley but also partially lifts SU_2^Λ symmetry.

Hidden SU_2^Λ symmetry of the dominant part of $\hat{H}$ in Eq. (4) enables us to classify the two-particle correlation functions, "Cooperons" which determine the interference correction to the conductivity, δg by pseudospin. Below, we show that δg is determined by the interplay of one pseudospin singlet (C^0) and three triplet ($C^{x,y,z}$) Cooperons, $\delta g \propto -C^0 + C^z + C^x + C^y$, some of which are suppressed due to a lower symmetry of the Hamiltonian in real graphene structures. That is, the "warping" term $\hat{h}_w$ and the disorder $\Sigma_s \Lambda_z u_{s,z}$ suppress intravalley Cooperons $C^{x,y}$ and wash out the Berry phase effect and WAL, whereas intervalley disorder $\Sigma_s \Lambda_{x(y)} u_{s,x(y)}(\mathbf{r})$ suppresses C^z and restores weak localization [9] of electrons, provided that their phase coherence is long. This results in a WL-type negative weak-field magnetoresistance in graphene, which is absent when the intervalley scattering time is long, as we discuss at the end of this Letter.

To describe quantum transport of 2D electrons in graphene we (a) evaluate the disorder-averaged one-particle Green functions, vertex corrections, Drude conductivity, and transport time; (b) classify Cooperon modes and derive equations for those which are gapless in the limit of purely potential disorder; (c) analyze "Hikami boxes" [9,10] for the weak localization diagrams paying attention to a peculiar form of the current operator for Dirac electrons and evaluate the interference correction to conductivity leading to the WL magnetoresistance. In these calculations, we treat trigonal warping $\hat{h}_w$ in the free-electron Hamiltonian Eqs. (1) and (4) perturbatively, assume that potential disorder $\hat{I}u(\mathbf{r})$ dominates in the elastic scattering rate, $\tau^{-1} \approx \tau_0^{-1} = \pi\gamma u^2/\hbar$, and take into account all other types of disorder when we determine the relaxation spectra of low-gap Cooperons.

(a) Standard methods of the diagrammatic technique for disordered systems [9,10] at $p_F v\tau \gg \hbar$ yield the disorder-averaged single particle Green's function,

$$\hat{G}^{R/A}(\mathbf{p}, \epsilon) = \frac{\epsilon_{R/A} + v\vec{\Sigma}\mathbf{p}}{\epsilon_{R/A}^2 - v^2 p^2}, \qquad \epsilon_{R/A} = \epsilon \pm \frac{1}{2} i\hbar\tau_0^{-1}.$$

The current operator, $\hat{\mathbf{v}} = v\vec{\Sigma}$, for the Dirac-type particles described in Eq. (1) is momentum independent. As a result, the current vertex $\tilde{v}_j$ ($j = x, y$), which enters the Drude conductivity, Fig. 1(a),

$$g_{jj} = \frac{e^2}{\pi\hbar} \int \frac{d^2p}{(2\pi)^2} \mathrm{Tr}\{\tilde{v}_j \hat{G}^R(\mathbf{p}, \epsilon)\hat{v}_j \hat{G}^A(\mathbf{p}, \epsilon)\},$$
$$= 4e^2\gamma D, \quad \text{with} \quad D = v^2\tau_0 \equiv \frac{1}{2} v^2 \tau_{\mathrm{tr}}, \tag{5}$$

is renormalized by vertex corrections in Fig. 1(b): $\tilde{\mathbf{v}} = 2\hat{\mathbf{v}} = 2v\vec{\Sigma}$. Here, Tr stands for the trace over the AB and valley indices. The transport time in graphene is twice the scattering time, $\tau_{\mathrm{tr}} = 2\tau_0$, due to the scattering anisotropy (lack of backskattering off a potential scatterer). This follows from the Einstein relation Eq. (5) (where spin degeneracy has been taken into account).

(b) The WL correction to the conductivity is associated with the disorder-averaged two-particle correlation function $C^{\xi\mu,\xi'\mu'}_{\alpha\beta,\alpha'\beta'}$ known as the Cooperon. It obeys the Bethe-Salpeter equation represented diagrammatically in Fig. 1(c). The shaded blocks in Fig. 1(c) are infinite series of ladder diagrams, while the dashed lines represent the correlator of the disorder in Eq. (4). Here, the valley indices ($\mathbf{K}_\pm$) of the Dirac-type electron are included as superscripts with incoming $\xi\mu$ and outgoing $\xi'\mu'$, and the sublattice (AB) indices as subscripts $\alpha\beta$ and $\alpha'\beta'$.

It is convenient to classify Cooperons in graphene as iso- and pseudospin singlets and triplets,

$$C^{l_1 l_2}_{s_1 s_2} = \tfrac{1}{4} \sum_{\alpha,\beta,\alpha',\beta',} \sum_{\xi,\mu,\xi',\mu',} (\Sigma_y \Sigma_{s_1} \Lambda_y \Lambda_{l_1})^{\xi\mu}_{\alpha\beta}$$
$$\times C^{\xi\mu,\xi'\mu'}_{\alpha\beta,\alpha'\beta'} (\Sigma_{s_2} \Sigma_y \Lambda_{l_2} \Lambda_y)^{\mu'\xi'}_{\beta'\alpha'}. \tag{6}$$

Such a classification of modes is permitted by the commutation of the iso- and pseudospin operators $\vec{\Sigma}$ and $\vec{\Lambda}$ in

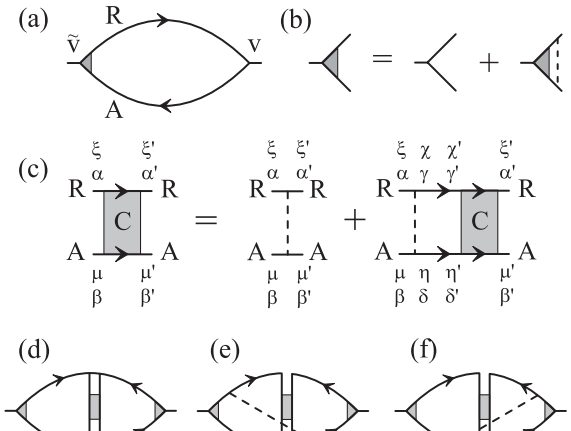

FIG. 1. (a) Diagram for the Drude conductivity with (b) the vertex correction. (c) Bethe-Salpeter equation for the Cooperon propagator with valley indices $\xi\mu\xi'\mu'$ and AB lattice indices $\alpha\beta\alpha'\beta'$. (d) Bare "Hikami box" relating the conductivity correction to the Cooperon propagator with (e) and (f) dressed "Hikami boxes." Solid lines represent disorder averaged $G^{R/A}$; dashed lines represent disorder.

Eqs. (2), (3), and (6), $[\Sigma_s, \Lambda_l] = 0$. To select the isospin-singlet ($s = 0$) and triplet ($s = x, y, z$) Cooperon components (scalar and vector representation of the group $\mathrm{SU}_2^{\Sigma} \equiv \{e^{ia\vec{n}\cdot\vec{\Sigma}}\}$), we project the incoming and outgoing Cooperon indices onto matrices $\Sigma_y\Sigma_{s_1}$ and $\Sigma_{s_2}\Sigma_y$, respectively. The pseudospin-singlet ($l = 0$) and triplet ($l = x, y, z$) Cooperons (scalar and vector representation of the "valley" group $\mathrm{SU}_2^{\Lambda} \equiv \{e^{ib\vec{n}\cdot\vec{\Sigma}}\}$) are determined by the projection of $C^{\xi\mu,\xi'\mu'}_{\alpha\beta,\alpha'\beta'}$ onto matrices $\Lambda_y\Lambda_{l_1}$ ($\Lambda_{l_2}\Lambda_y$) and are accounted for by superscript indices in $C^{l_1 l_2}_{s_1 s_2}$.

For disorder $\hat{I}u(\mathbf{r})$, the equation in Fig. 1(c) is

$$C^{l_1 l_2}_{s_1 s_2}(\mathbf{q}) = \tau_0 \delta^{l_1 l_2}\delta_{s_1 s_2} + \frac{1}{4\pi\gamma\tau_0\hbar}\sum_{s,l} C^{l l_2}_{s s_2}(\mathbf{q}) \int \frac{d^2p}{(2\pi)^2}\,\mathrm{Tr}\{\Sigma_s\Sigma_y\Lambda_l\Lambda_y[\hat{G}^R_{\mathbf{p},\hbar\omega+\epsilon}]^{\mathrm{t}}\Lambda_y\Lambda_{l_1}\Sigma_y\Sigma_{s_1}\hat{G}^A_{\hbar\mathbf{q}-\mathbf{p},\epsilon}\}.$$

It leads to a series of coupled equations for the Cooperon matrix $\mathbf{C}^l$ with components $C^{ll}_{ss'}$. It turns out that for potential disorder $\hat{I}u(\mathbf{r})$ isospin-singlet modes C^{ll}_{00} are gapless in all (singlet and triplet) pseudospin channels, whereas triplet modes C^{ll}_{xx} and C^{ll}_{yy} have relaxation gaps $\Gamma^l_x = \Gamma^l_y = \frac{1}{2}\tau_0^{-1}$ and C^{ll}_{zz} have gaps $\Gamma^l_z = \tau_0^{-1}$. When obtaining the diffusion equations for the Cooperons using the gradient expansion of the Bethe-Salpeter equation, we take into account its matrix structure. The matrix equation for each Cooperon matrix $\mathbf{C}^l$, where $l = 0, x, y, z$, has the form

$$\begin{pmatrix} \frac{1}{2}v^2\tau_0 q^2 + \Gamma^l_0 - i\omega & \frac{-i}{2}vq_x & \frac{-i}{2}vq_y & 0 \\ \frac{-i}{2}vq_x & \frac{1}{2}\tau_0^{-1} & 0 & 0 \\ \frac{-i}{2}vq_y & 0 & \frac{1}{2}\tau_0^{-1} & 0 \\ 0 & 0 & 0 & \tau_0^{-1} \end{pmatrix}\mathbf{C}^l = \hat{1}.$$

After the isospin-triplet modes were eliminated, the diffusion operator for each of the four gapless or low-gap modes $C^l_0 = C^{ll}_{00}$ becomes $Dq^2 - i\omega + \Gamma^l_0$, where $D = \frac{1}{2}v^2\tau_{\mathrm{tr}} = v^2\tau_0$.

Symmetry-breaking perturbations lead to relaxation gaps Γ^l_0 in the otherwise gapless pseudospin-triplet components, C^x_0, C^y_0, C^z_0 of the isospin-singlet Cooperon, though they do not generate a relaxation of the pseudospin-singlet C^0_0 protected by the time-reversal symmetry of the Hamiltonian (4). We include all scattering mechanisms described in Eq. (4) in the corresponding disorder correlator (dashed line) on the right-hand side of the Bethe-Salpeter equation and in the scattering rate in the disorder-averaged $G^{R/A}$, as $\tau_0^{-1} \to \tau^{-1} = \tau_0^{-1} + \sum_{sl}\tau_{sl}^{-1}$. For simplicity, we assume that different types of disorder are uncorrelated, $\langle u_{s,l}(\mathbf{r})u_{s',l'}(\mathbf{r}')\rangle = u^2_{sl}\delta_{ss'}\delta_{ll'}\delta(\mathbf{r}-\mathbf{r}')$ and, on average, isotropic in the x-y plane: $u^2_{xl} = u^2_{yl} \equiv u^2_{\perp l}$, $u^2_{sx} = u^2_{sy} \equiv u^2_{s\perp}$. We parametrize them by scattering rates $\tau_{sl}^{-1} = \pi\gamma u^2_{sl}/\hbar$, where $\tau_{sx}^{-1} = \tau_{sy}^{-1} \equiv \tau_{s\perp}^{-1}$ and $\tau_{xl}^{-1} = \tau_{yl}^{-1} \equiv \tau_{\perp l}^{-1}$ due to the x-y plane isotropy of disorder, which are combined into the intervalley scattering rate τ_i^{-1} and the intravalley rate τ_z^{-1}, as

$$\tau_i^{-1} = 4\tau_{\perp\perp}^{-1} + 2\tau_{z\perp}^{-1}, \qquad \tau_z^{-1} = 4\tau_{\perp z}^{-1} + 2\tau_{zz}^{-1}. \tag{7}$$

The trigonal warping term, $\hat{h}_w$ in the Hamiltonian (1) plays a crucial role for the interference effects since it breaks the $\mathbf{p} \to -\mathbf{p}$ symmetry of the Fermi lines within each valley: $\epsilon(\mathbf{K}_{\pm}, -\mathbf{p}) \neq \epsilon(\mathbf{K}_{\pm}, \mathbf{p})$, while $\epsilon(\mathbf{K}_{\pm}, -\mathbf{p}) = \epsilon(\mathbf{K}_{\mp}, \mathbf{p})$ [8]. It has been noticed [16] that such a deformation of a Fermi line of 2D electrons suppresses Cooperons. As $\hat{h}_w$ has a similar effect, it suppresses the pseudospin-triplet intravalley components C^x_0 and C^y_0, at the rate

$$\tau_w^{-1} = 2\tau_0(\epsilon^2\mu/\hbar v^2)^2. \tag{8}$$

However, since warping has an opposite effect on valleys $\mathbf{K}_+$ and $\mathbf{K}_-$, it does not cause gaps in the intervalley Cooperons C^0_0 (the only true gapless Cooperon mode) and C^z_0.

Altogether, the relaxation of modes C^l_0 can be described by the following combinations of rates:

$$\Gamma^0_0 = 0, \qquad \Gamma^z_0 = 2\tau_i^{-1},$$
$$\Gamma^x_0 = \Gamma^y_0 = \tau_w^{-1} + \tau_z^{-1} + \tau_i^{-1} \equiv \tau_*^{-1}.$$

In the presence of an external magnetic field, $\mathbf{B} = \mathrm{rot}\mathbf{A}$, and inelastic decoherence, τ_φ^{-1}, equations for $C^l_0 = C^{ll}_{00}$ read

$$[D(i\nabla + \frac{2e}{c\hbar}\mathbf{A})^2 + \Gamma^l_0 + \tau_\varphi^{-1} - i\omega]C^l_0(\mathbf{r},\mathbf{r}') = \delta(\mathbf{r}-\mathbf{r}').$$

(c) Because of the momentum-independent form of the current operator $\tilde{\mathbf{v}} = 2v\vec{\Sigma}$, the WL correction to conductivity δg includes two additional diagrams, Fig. 1(e) and 1(f) besides the standard diagram shown in Fig. 1(d). Each of the diagrams in Fig. 1(e) and 1(f) (not included in the analysis in Ref. [11]) produces a contribution equal to $(-\frac{1}{4})$ of that in Fig. 1(d). This partial cancellation, together with a factor of 4 from the vertex corrections and a factor of 2 from spin degeneracy, leads to

$$\delta g = \frac{2e^2D}{\pi\hbar}\int\frac{d^2q}{(2\pi)^2}(C^x_0 + C^y_0 + C^z_0 - C^0_0). \tag{9}$$

Using Eq. (9), we find the $B = 0$ temperature dependent correction, $\delta\rho$, to the graphene sheet resistance,

$$\frac{\delta\rho(0)}{\rho^2} = -\delta g = \frac{e^2}{\pi h}\left[\ln\left(1 + 2\frac{\tau_\varphi}{\tau_i}\right) - 2\ln\frac{\tau_\varphi/\tau_{\mathrm{tr}}}{1+\frac{\tau_\varphi}{\tau_*}}\right], \tag{10}$$

and evaluate magnetoresistance, $\rho(B) - \rho(0) \equiv \Delta\rho(B)$,

$$\Delta\rho(B) = -\frac{e^2\rho^2}{\pi h}\left[F\left(\frac{B}{B_\varphi}\right) - F\left(\frac{B}{B_\varphi + 2B_i}\right) - 2F\left(\frac{B}{B_\varphi + B_*}\right)\right],$$
$$F(z) = \ln z + \psi\left(\frac{1}{2} + \frac{1}{z}\right), \quad B_{\varphi,i,*} = \frac{\hbar c}{4De}\tau^{-1}_{\varphi,i,*}. \tag{11}$$

Here, ψ is the digamma function, and the decoherence $\tau_\varphi^{-1}(T)$ determines the curvature of $\Delta\rho(B)$ at $B \lesssim B_\varphi$.

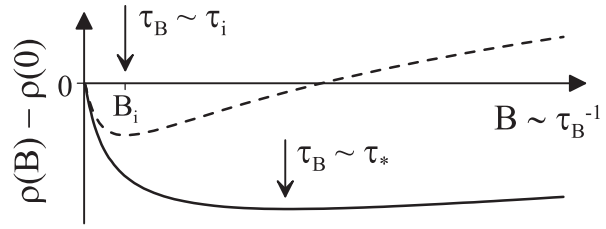

FIG. 2. MR expected in a phase-coherent graphene $\tau_\varphi \gg \tau_i$: with τ_z, $\tau_w \gg \tau_i$ (dashed line) and $\tau_* \ll \tau_i$ (solid line). In the case of $\tau_\varphi < \tau_i$, $\delta\rho = 0$, so that $\Delta\rho(B) = 0$.

Equations (10) and (11) represent the main result of this Letter. They show that in graphene samples with the intervalley time shorter than the decoherence time, $\tau_\varphi > \tau_i$, the quantum correction to the conductivity has the WL sign. Such behavior is expected in graphene tightly coupled to the substrate (which generates atomically sharp scatterers). Figure 2 illustrates the corresponding MR in two regimes: $B_* \sim B_i$ (τ_z, $\tau_w \gg \tau_i$) and $B_* \gg B_i$ ($\tau_* \ll \tau_i$). In both cases, the low-field MR at $B < B_i$ is negative (for $B_* \sim B_i$, the MR changes sign at $B \sim B_i$). A dashed line shows what one would get upon neglecting the effect of warping; the solid curve shows the MR behavior in graphene with a high carrier density, where the effect of warping is strong and leads to a fast relaxation of intravalley Cooperons, at the rate described in Eq. (10). Then, in Eqs. (10) and (11) $\tau_* \approx \tau_w \ll \tau_i < \tau_\varphi$ and $B_* \gg B_i$, which determines MR of a distinctly WL type. Note that in the latter case, MR is saturated at $B \sim B_i$, in contrast to the WL MR in conventional electron systems, where the logarithmic field dependence extends into the field range of $\hbar c/4De\tau_{\rm tr}$. In a sheet loosely attached to a substrate (or suspended), the intervalley scattering time may be longer than the decoherence time, $\tau_i > \tau_\varphi > \tau_w$ ($B_i < B_\varphi < B_*$). In this case, C_0^z in Eq. (11) is effectively gapless and cancels C_0^0, whereas trigonal warping suppresses the modes C_0^x and C_0^y, so that $\delta g = 0$ and MR displays neither WL nor WAL behavior: $\Delta\rho(B) = 0$.

Equation (11) explains why in the recent experiments on quantum transport in graphene [17] the observed low-field MR displayed a suppressed WL behavior rather than WAL. For all electron densities in the samples studied in [17] the estimated warping-induced relaxation time is rather short, $\tau_w/\tau_{\rm tr} \sim 5$–$30$, $\tau_w < \tau_\varphi$, which excluded any WAL. Moreover, the observation [17] of a suppressed WL MR in devices with a tighter coupling to the substrate agrees with the behavior expected in the case of sufficient intervalley scattering, $\tau_i < \tau_\varphi$, whereas the absence of any WL MR, $\Delta\rho(B) = 0$, for a loosely coupled graphene sheet is what we predict for samples with a long intervalley scattering time, $\tau_i > \tau_\varphi$.

In a narrow wire with the transverse diffusion time $L_\perp^2/D \ll \tau_i$, τ_*, τ_φ edges scatter between valleys [18]. Thus, we estimate $\Gamma_0^l \sim \pi^2 D/L_\perp^2$ for the pseudospin triplet in a wire, whereas the singlet C_0^0 remains gapless. This yields negative MR for $B \lesssim 2\pi B_\perp$, $B_\perp \equiv \hbar c/eL_\perp^2$:

$$\frac{\Delta\rho_{\rm wire}(B)}{\rho^2} = \frac{2e^2 L_\varphi}{h}\left[\frac{1}{\sqrt{1+\frac{1}{3}B^2/B_\varphi B_\perp}} - 1\right]. \quad (12)$$

Equations (10)–(12) completely describe the WL effect in graphene and explain how the WL magnetoresistance reflects the degree of valley symmetry breaking. They show that, despite the chiral nature of electrons in graphene suggestive of antilocalization, their long-range propagation in a real disordered material or a narrow wire does not manifest the chirality.

We thank I. Aleiner, V. Cheianov, A. Geim, P. Kim, O. Kashuba, and C. Marcus for discussions. This project has been funded by the EPSRC Grant No. EP/C511743.

[1] Y. Zheng and T. Ando, Phys. Rev. B **65**, 245420 (2002); V. Gusynin and S. Sharapov, Phys. Rev. Lett. **95**, 146801 (2005); A. Castro Neto, F. Guinea, and N. Peres, Phys. Rev. B **73**, 205408 (2006).
[2] T. Ando, T. Nakanishi, and R. Saito, J. Phys. Soc. Jpn. **67**, 2857 (1998).
[3] E. McCann and V. I. Fal'ko, Phys. Rev. Lett. **96**, 086805 (2006).
[4] V. Cheianov and V. I. Fal'ko, Phys. Rev. B **74**, 041403 (2006).
[5] K. S. Novoselov *et al.*, Nature (London) **438**, 197 (2005); Nature Phys. **2**, 177 (2006).
[6] Y. Zhang *et al.*, Phys. Rev. Lett. **94**, 176803 (2005); Nature (London) **438**, 201 (2005).
[7] T. Ando, J. Phys. Soc. Jpn. **74**, 777 (2005).
[8] Here, $\mathbf{K}_\pm = \pm(\frac{2}{3}ha^{-1}, 0)$, a is the lattice constant.
[9] B. L. Altshuler, D. Khmelnitski, A. I. Larkin, and P. A. Lee, Phys. Rev. B **22**, 5142 (1980).
[10] S. Hikami, A. I. Larkin, and N. Nagaosa, Prog. Theor. Phys. **63**, 707 (1980).
[11] H. Suzuura and T. Ando, Phys. Rev. Lett. **89**, 266603 (2002).
[12] D. V. Khveshchenko, Phys. Rev. Lett. **97**, 036802 (2006).
[13] The group U_4 can be described using 16 generators $\hat{I}$, Σ_s, Λ_l, $\Sigma_s\Lambda_l$; s, $l = x$, y, x.
[14] In the basis $\Phi = [\phi_{\mathbf{K}_+,A}, \phi_{\mathbf{K}_+,B}, \phi_{\mathbf{K}_-,B}, \phi_{\mathbf{K}_-,A}]$, time reversal of an operator W is $T(\hat{W}) = (\Pi_x \otimes \sigma_x)W^*(\Pi_x \otimes \sigma_x)$, and $T(\Sigma_s) = -\Sigma_s$, $T(\Lambda_l) = -\Lambda_l$, $T(\Sigma_s\Lambda_l) = \Sigma_s\Lambda_l$.
[15] E. Fradkin, Phys. Rev. B **33**, 3257 (1986); N. Shon and T. Ando, J. Phys. Soc. Jpn. **67**, 2421 (1998); E. McCann and V. I. Fal'ko, Phys. Rev. B **71**, 085415 (2005); M. Foster and A. Ludwig, Phys. Rev. B **73**, 155104 (2006).
[16] V. I. Fal'ko and T. Jungwirth, Phys. Rev. B **65**, 081306 (2002); D. Zumbuhl *et al.*, Phys. Rev. B **69**, 121305 (2004).
[17] S. Morozov *et al.*, Phys. Rev. Lett. **97**, 016801 (2006).
[18] E. McCann and V. I. Fal'ko, J. Phys. Condens. Matter **16**, 2371 (2004).